Arabian Journal of Chemistry (2019) **12**, 3463–3478

King Saud University

Arabian Journal of Chemistry

www.ksu.edu.sa
www.sciencedirect.com

ORIGINAL ARTICLE

Solvatochromism and azo–hydrazo tautomerism of novel arylazo pyridone dyes: Experimental and quantum chemical study

Ismail Ajaj [a], Fathi H. Assaleh [b], Jasmina Markovski [c], Milica Rančić [d,*], Danijela Brković [e], Miloš Milčić [f], Aleksandar D. Marinković [a]

[a] *Faculty of Technology and Metallurgy, University of Belgrade, Karnegijeva 4, 11120 Belgrade, Serbia*
[b] *Faculty of Science, Chemistry Department, Zawia University, P.O. Box 16168, Zawia, Libya*
[c] *Vinča Institute, University of Belgrade, 11000 Belgrade, Serbia*
[d] *Faculty of Forestry, University of Belgrade, Kneza Višeslava 1, 11030 Belgrade, Serbia*
[e] *Innovation Center, Faculty of Technology and Metallurgy, University of Belgrade, Karnegijeva 4, 11120 Belgrade, Serbia*
[f] *Faculty of Chemistry, University of Belgrade, Studentski trg 12-16, 11000 Belgrade, Serbia*

Received 13 January 2015; accepted 27 August 2015
Available online 22 October 2015

KEYWORDS

Arylazo pyridone dye;
UV–Vis spectra;
Solvatochromism;
Azo–Hydrazo tautomerism

Abstract The state of the tautomeric equilibria of eleven arylazo pyridone dyes was evaluated from UV–Vis absorption spectra with the aid of the quantum mechanical modeling. NMR analysis and theoretical calculations, by using PCM/ωB97X-D/6-311G(d,p) method, confirmed that prepared compounds exist mainly in **Hydrazo** form. Internal hydrogen bonding in **Hydrazo** tautomer, analyzed by AIM topological analysis and total electron density at the bond critical point (BCP), confirmed a presence of strong hydrogen bond which contributes to higher stability of **Hydrazo** form. Linear solvation energy relationships (LSERs) rationalized solvent influence on solvatochromism of all compounds in **Hydrazo** form and K_T by using Kamlet–Taft model. Linear free energy relationships (LFERs) were applied to the substituent-induced NMR chemical shifts (*SCS*) using SSP (single substituent parameter) and DSP (dual substituent parameter) model. Density plots over the highest occupied (HOMO) and lowest unoccupied molecular orbitals (LUMO) energy surface provide information on the charge transfer during excitation. The molecular electrostatic potential (MEP)

* Corresponding author. Tel.: +381 11 3053 893; fax: +381 11 2547 478.
E-mail address: milica.rancic@sfb.bg.ac.rs (M. Rančić).
Peer review under responsibility of King Saud University.

Production and hosting by Elsevier

http://dx.doi.org/10.1016/j.arabjc.2015.08.029

surface map was plotted over the optimized geometry of the molecules in order to visualize electron density distribution and explain origin of solvent/solute interactions.

1. Introduction

Azo dyes containing heterocycle unit have attracted considerable attention because of their importance for chemistry of dyes and dyeing process (Peng et al., 1990, 1991; Yazdanbakhsh et al., 2007; Zhang et al., 2005; Yen and Wang, 2004; Hosseinnezhad et al., 2019). Apart from their conventional application in textile dyeing, cosmetics, leather and food industry (Zöllinger, 2003), azo dyes have been recently used in biological and medical studies (Isak et al., 2000), optical recording (Geng et al., 2004), dye-sensitized solar cells (Li et al., 2010) and high technology products and innovations (Tao et al., 1999). Disperse dyes containing pyridone unit as a coupling component possess a great significance for dyestuff industry due to their excellent coloration features, simplicity of preparation, good light and wash fastness properties (Zöllinger, 2003). Their physico-chemical properties, including optical storage capacity, optical switching, holography and non-linear optical properties make them promising candidates for photoactive materials (He et al., 2000).

The physico-chemical properties of arylazo pyridones are closely related to their **Azo–Hydrazo** tautomerism. Since the tautomers have different technical properties and dyeing performances, studying the state of tautomeric equilibria is important from both theoretical and practical point of view. Despite numerous publications which have focused on the industrial applications, surprisingly few studies were published on conformation originated from the isomerization/tautomerism or the stereochemistry of these molecules (Wang and Wang, 1990; Peng et al., 1991; Ertan et al., 1995; Uščumlić et al., 2004; Mijin et al., 2006). The small free energy difference between tautomers makes them sensitive to the influence of environment (*e.g.* pH, temperature, solvent polarity and the ability of solvents to hydrogen bond with each tautomer) and substituent effects (their position in the ring and their electronic effects, and inter- and intra-molecular interactions) (Antonov, 2013).

An investigation of the spectral data generally pointed out that the tautomeric equilibrium of arylazo pyridone dyes is shifted to the hydrazo tautomeric form in solid state. In different solvents, the equilibrium predominantly favors the hydrazo form and depends on the dye structure and the solvent used (Cee et al., 1988; Ertan et al., 1995; Uščumlić et al., 2004). Previous investigations of substituted arylazo pyridones (Alimmari et al., 2012, 2013) have also shown that the equilibrium between the two tautomers is influenced by the structure of the compounds and the solvent used. The introduction of electron-attracting or electron-donating substituents to the *para* or *ortho* positions of diazo component of an azo pyridone dye, has resulted in additive or subtractive color shifts and fading rates which depend on the nature and the position of the substituents (Wang and Wang, 1990).

A series of eleven arylazo pyridone dyes were synthesized by coupling of 3- or 4-substituted benzene diazonium salt with tautomeric mixture of 6(2)-hydroxy-4-methyl-2(6)-oxo-1-phenyl-1,2(1,6)-dihydropyridine-3-carbonitriles (pyridone **a** and **b**; Fig. 1) (Ajaj et al., 2013). The reaction pathways take place *via* equilibration of the azo forms: **Azo**/**b** – (*E*)-2-hydroxy-4-methyl-5-((3- or 4-substituted phenyl)diazenyl)-6-oxo-1-phenyl-1,6-dihydropyridine-3-carbonitrile and **Azo**/**a** – (*E*)-6-hydroxy-4-methyl-5-((3- or 4-substituted phenyl)diazenyl)-2-oxo-1-phenyl-1,2-dihydropyridine-3-carbonitrile with the main reaction product **Hydrazo** form: (*Z*)-4-methyl-5-[2-(3 or 4-substituted phenyl)hydrazono]-2,6-dioxo-1-phenyl-1,2,5,6-tetrahydropyridine-3-carbonitrile dyes at 0–5 °C, which is presented in Fig. 1.

Experimental and theoretical data of the tautomeric forms were considered. The state of the tautomeric equilibria of eleven arylazo pyridone dyes was evaluated from UV–Vis spectra. Due to overlapping of the absorption bands, the applied methodology for resolution of UV–Vis spectra was based on certain approximations (Antonov and Stoyanov, 1995). The algorithm applied for evaluation of the state of tautomeric equilibria was described elsewhere (Ajaj et al., 2013; Antonov and Stoyanov, 1993). A detail study of the relative stability of tautomers requires the use of computational techniques to support the experimental findings. Thus, geometries and electronic structure of arylazo pyridone dyes were obtained from DFT calculations.

The UV–Vis and NMR data were analyzed by the use of LSER and LFER models, respectively, in order to evaluate the influence of solvent/solute interactions and substituent effects on tautomeric equilibria (Reichardt, 2003). Quantification of the solvent effects: dipolarity/polarizability and the hydrogen-bonding ability on the UV spectral shifts, *i.e.* ν_{max}, was interpreted by means of the Kamlet–Taft (LSER) Eq. (1) (Kamlet et al., 1981):

$$\nu_{max} = \nu_o + s\pi^* + b\beta + a\alpha \quad (1)$$

where ν_{max} is substituent-dependent values, *i.e.*, absorption frequencies, π^* is an index of the solvent dipolarity/polarizability; α is a measure of the solvent bond acceptor (HBA) basicity; β is a measure of the solvent hydrogen-bond donor (HBD) acidity and ν_o is the regression value in cyclohexane as reference solvent. The solvent parameters used in Eq. (1) are given in Table S1. The regression coefficients s, b and a in Eq. (1) measure the relative susceptibilities of the absorption frequencies to the indicated solvent parameters.

In the second part of the work, LFER analysis was applied to the UV and NMR data in the studied compounds (Fig. 1). The transmission of polar (field/inductive) and resonance effects from the substituent (X) to the carbon atoms of interest was studied using Eqs. (2) and (3):

$$s = \rho\sigma + h \quad (2)$$

$$s = \rho_I\sigma_I + \rho_R\sigma_R + h \quad (3)$$

where s are substituent-dependent values: substituent induced chemical shift (*SCS*) or absorption frequencies (ν_{max}); ρ is a

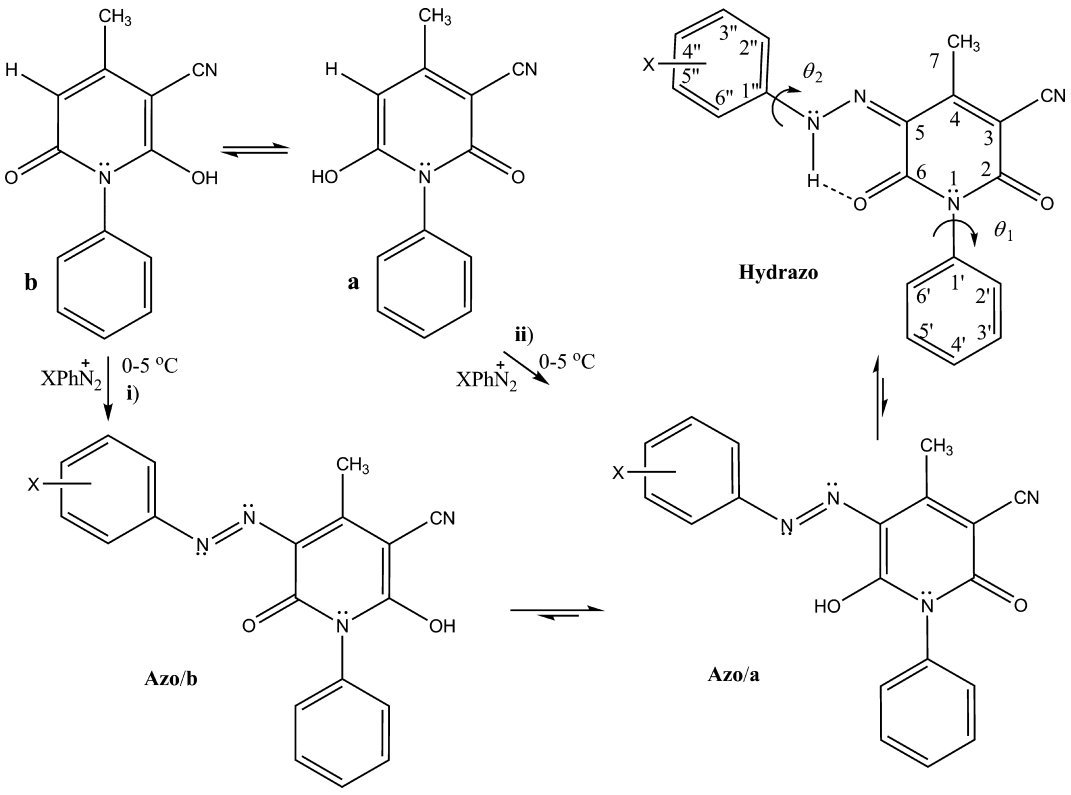

Figure 1 The proposed reaction pathways of the diazotization of tautomeric pyridone **a** and **b** form via equilibration of azo forms (**Azo/b** and **Azo/a**) and **Hydrazo** form of arylazo pyridone dyes at 0–5 °C (Ajaj et al., 2013).

proportionality constant (reaction constant) reflecting the sensitivity of the spectral data to the substituent effects; σ, σ_I and σ_R are the substituent constants, and h is the intercept (*i.e.*, it describes the unsubstituted member of the series) (Hammett, 1937; Exner, 1972; Hansch et al., 1995). Single substituent parameter Eq. (2) (SSP; the Hammett Equation) attributes the observed substituent effect to an additive blend of polar and π-delocalization effects given as corresponding the σ values. In dual-substituent parameter (DSP) Eq. (3) (the Extended Hammett Equation), s are correlated by a linear combination of inductive (σ_I) and various resonance scales (σ_R^0, σ_R and σ_R^+), depending on the electronic demand of the atom under study. Calculated values ρ_I and ρ_R, are relative measures of the transmission of the inductive and resonance effects.

The transmission of substituent effects, *i.e.* LFER study, was discussed in relation to the geometry of molecules. DFT method was also applied for evaluation of HOMO–LUMO energy gaps and Molecule Electrostatic Potential (MEP) maps.

2. Experimental

2.1. Materials and methods

Details on materials and general method for preparation and purification procedure of arylazo pyridone dyes were described in detail in Supplementary material. Atom numbering used in NMR calculations and assignment of chemical shifts of arylazo pyridone dyes are given in Fig. S1. Yield and melting points of obtained arylazo pyridone dyes are given in Table 1.

Table 1 Yields and melting points of the obtained arylazo pyridone dyes.

Comp.	Substitute (X)	Formula	Yield/%	M.p./°C
1	H	$C_{19}H_{14}N_4O_2$	78	271–3
2	4-CH_3	$C_{20}H_{16}N_4O_2$	63	229–31
3	4-OCH_3	$C_{20}H_{16}N_4O_3$	66	247–9
4	4-NO_2	$C_{19}H_{13}N_5O_4$	64	> 300
5	4-F	$C_{19}H_{13}N_4O_2F$	65	256–8
6	4-Br	$C_{19}H_{13}N_4O_2Br$	60	275–7
7	4-I	$C_{19}H_{13}N_4O_2I$	71	273–5
8	4-Cl	$C_{19}H_{13}N_4O_2Cl$	69	226–8
9	3-CF_3	$C_{20}H_{13}N_4O_2F_3$	76	259–61
10	3-Br	$C_{19}H_{13}N_4O_2Br$	66	278–80
11	3-Cl	$C_{19}H_{13}N_4O_2Cl$	72	235–7

The UV absorption spectra were recorded in the range from 200 to 600 nm in seventeen solvents of different polarity at 25 °C using UV–Vis Shimadzu 1700A spectrophotometer. Three measurements were performed and mean value was presented. Spectra were recorded at variable conditions, temperature and concentration, in order to study their effect on the solvatochromism and tautomeric equilibria of investigated compounds. Concentration was changed in the range from 1.00×10^{-4} to 1.00×10^{-7} mol dm^{-3}, and at temperature of 25, 35, 45 and 55 ± 0.1 °C. Second and fourth derivatives spectroscopy are explained in Supplementary material. The correlations of the absorption frequencies ν_{max}, by applying LSER and LFER principles, were carried out by means of multiple linear regression analysis, and all correlations fit at

the 95% confidence level. The standard deviation for correlation and correlation parameter is presented. The Kamlet–Taft solvent parameters are taken from the literature (Kamlet et al., 1983), as well as substituent constants used in LSER and LFER correlations (Hansch et al., 1995).

2.2. Results of the characterization of arylazo pyridone dyes *1*–*11*

^{1}H and ^{13}C NMR, FTIR data and results of elemental analysis of known compounds **1**, **2**, **4** and **8** are given in Supplementary material, while data for newly synthesized compounds are as follows:

(Z)-4-methyl-5-[2-phenylhydrazono]-2,6-dioxo-1-phenyl-1,2,5,6-tetrahydro-3-carbonitriles (**1**, $C_{19}H_{14}N_4O_2$). Yellow-orange powder; yield 78%, m.p.: 271–3 °C [lit. m.p. > 300 °C] (Mohareb and Ibrahim, 1989).

(Z)-4-methyl-5-[2-(4-methylphenyl)hydrazono]-2,6-dioxo-1-phenyl-1,2,5,6-tetrahydro-3-carbonitriles (**2**, $C_{20}H_{16}N_4O_2$).

Brownish powder; yield 63%, m.p.: 229–31 °C [lit. m.p. 225 °C] (Shams et al., 2008).

(Z)-4-methyl-5-[2-(4-methoxyphenyl)hydrazono]-2,6-dioxo-1-phenyl-1,2,5,6-tetrahydro-3-carbonitriles (**3**, $C_{20}H_{16}N_4O_3$).

Red powder; yield 66%, m.p.: 247–9 °C.

^{1}H NMR (500 MHz, DMSO-d_6): δ = 2.50 (s, 3H, 4-CH_3), 3.79 (s, 3H, 4″-OCH_3), 7.29–7.33 (m, 2H, 2′-H, 6′-H), 7.48–7.52 (m, 3H, 4′-H, 3′-H, 5′-H), 7.06 (AA′XX′, J = 8.8 Hz, 2H, C_6H_4—OCH_3), 7.69 (AA′XX′, J = 8.8 Hz, 2H, C_6H_4—OCH_3), 14.69 (s, 1H, N—H) ppm; ^{13}C NMR (125 MHz, DMSO-d_6): δ = 16.6 (C7), 55.7 (4″-OCH_3), 99.5 (C3), 115.3 (C≡N), 119.4 (C2″, C6″), 122.6 (C5), 128.7 (C4′), 128.8 (C3″, C5″), 129.0 (C3′, C5′), 129.1 (C2′, C6′), 134.4 (C1′), 134.8 (C1″) 139.1 (C4″), 158.9 (C2), 159.7 (C4), 160.8 (C6) ppm. IR (KBr): $\bar{\nu}$ = 637, 671, 702, 763, 832, 1009, 1090, 1211, 1278, 1397, 1418, 1508, 1585 1638, 1686 (C═O), 2222 (C≡N), 2924, 3446 (O—H) cm^{-1}. Elemental Analysis:

Calculated: %C 66.66, %H 4.48, %N 15.55, %O 13.32.

Found: %C 66.67, %H 4.46, %N 15.56, %O 13.31.

(Z)-4-methyl-5-[2-(4-nitrophenyl)hydrazono]-2,6-dioxo-1-phenyl-1,2,5,6-tetrahydro-3-carbonitriles (**4**, $C_{19}H_{13}N_5O_4$).

Red dark powder; yield 64%, m.p.: > 300 °C [lit. m.p. > 300 °C] (Ajaj et al., 2013).

(Z)-4-methyl-5-[2-(4-fluorophenyl)hydrazono]-2,6-dioxo-1-phenyl-1,2,5,6-tetrahydro-3-carbonitriles (**5**, $C_{19}H_{13}N_4O_2F$).

Yellow powder; yield 65%, m.p.: 265–8 °C.

^{1}H NMR (500 MHz, DMSO-d_6): δ = 2.61 (s, 3H, 4-CH_3), 7.30–7.35 (m, 4H, 2′-H, 3′-H, 5′-H, 6′-H), 7.44–7.47 (m, 1H, 4′-H), 7.49–7.52 (m, 2H, 2″-H, 6″-H), 7.76–7.79 (3″-H, 5″-H), 14.5 (s, 1H, N—H) ppm; ^{13}C NMR (125 MHz, DMSO-d_6): δ = 16.5 (C7), 100.7 (C3), 115.1 (C≡N), 116.54 116.72 (C2″, C6″), 119.4, 119.6 (C3″, C5″), 123.4 (C5), 128.5 (C4′), 128.8 (C3′, C5′), 129.0 (C2′, C6′), 134.1 (C1′), 137.9 (C4″), 159.6 (C1″), 159.7 (C2), 160.1 (C4), 160.4 (C6) ppm. IR (KBr): $\bar{\nu}$ = 635, 670, 692, 736, 749, 770, 791, 837, 871, 954, 1033, 1073, 1100, 1152, 1206, 1234, 1288, 1333, 1398, 1425, 1447, 1508, 1578, 1638, 1680 (C═O), 2221 (C≡N), 3075, 3448 (O—H) cm^{-1}. Elemental Analysis:

Calculated: %C 65.51, %H 3.76, %N 16.08, %O 9.19, %F 5.45.

Found: %C 65.49, %H 3.72, %N 16.05, %O 9.17, %F 5.42.

(Z)-4-methyl-5-[2-(4-bromophenyl)hydrazono]-2,6-dioxo-1-phenyl-1,2,5,6-tetrahydro-3-carbonitriles (**6**, $C_{19}H_{13}N_4O_2$ Br).

Red powder; yield 60%, m.p.: 275–7 °C.

^{1}H NMR (500 MHz, DMSO-d_6): δ = 2.61 (s, 3H, 4-CH_3), 7.27–7.33 (m, 3H, 4′-H, 2″-H, 6″-H), 7.46–7.53 (m, 4H, 2′-H, 6′-H, 5′-H, 3′-H), 7.647–7.69 (m, 2H, 3″-H, 5″-H), 14.35 (s, 1H, N—H) ppm; ^{13}C NMR (125 MHz, DMSO-d_6): δ = 16.4 (C7), 101.3 (C3), 114.9 (C≡N), 119.0 (C2″, C6″), 123.7 (C5), 128.1 (C4′), 128.5, 128.6 (C3″, C5″), 128.8 (C3′, C5′), 129.3 (C2′, C6′), 132.3 (C1′), 140.4 (C1″), 152.3 (C4″), 159.4 (C2), 159.9 (C4), 160.4 (C6) ppm. IR (KBr): $\bar{\nu}$ = 691, 667, 700, 755, 771, 796, 825, 831, 953, 1006, 1169, 1172, 1243, 1275, 1301, 1391, 1437, 1479, 1505, 1593, 1638, 1689 (C═O), 2219 (C≡N), 2923, 3070, 3116, 3435 (O—H) cm^{-1}. Elemental Analysis:

Calculated: %C 5576, %H 3.20, %N 13.69, %O 7.82, %Br 19.53.

Found: %C 60.73, %H 3.18, %N 13.71, %O 7.81, %Br 19.50.

(Z)-4-methyl-5-[2-(4-iodophenyl)hydrazono]-2,6-dioxo-1-phenyl-1,2,5,6-tetrahydro-3-carbonitriles (**7**, $C_{19}H_{13}N_4O_2I$).

Red powder; yield 71%, m.p.: 273–5 °C.

^{1}H NMR (500 MHz, DMSO-d_6): δ = 1.89 (s, 3H, 4-CH_3), 7.29–7.33 (d, 2H, 2″-H, 6″-H), 7.48–7.52 (m, 5H, 2′-H, 3′-H, 4′-H, 5′-H, 6′-H), 7.31–7.79 (m, 2H, 3″-H, 5″-H), 14.29 (s, 1H, N—H) ppm; ^{13}C NMR (125 MHz, DMSO-d_6): δ = 16.7 (C7), 92.1 (C4″), 101.5 (C3), 115.2 (C≡N), 119.6 (C2″, C6″), 124.0 (C5), 128.6 (C4′), 128.8 (C3″, C5″), 129.0 (C2′, C6′), 129.21 (C3′, C5′), 138.5 (C1″), 141.2 (C1′), 159.8 (C2), 160.7 (C4), 162.4 (C6) ppm. IR (KBr): $\bar{\nu}$ = 694, 771, 953, 1001, 1210, 1273, 1393, 1413, 1508, 1576 1638, 1690 (C═O), 2219 (C≡N), 3452 (O—H) cm^{-1}. Elemental Analysis:

Calculated: %C 50.05, %H 2.87, %N 12.28, %O 7.01, %I 27.82.

Found: %C 50.03, %H 2.85, %N 12.30, %O 7.02, %I 27.83.

(Z)-4-methyl-5-[2-(4-clorophenyl)hydrazono]-2,6-dioxo-1-phenyl-1,2,5,6-tetrahydro-3-carbonitriles (**8**, $C_{19}H_{13}N_4O_2Cl$).

Brownish powder; yield 69%, m.p.: 226–8 °C [lit. m.p. 150 °C] (Shams et al., 2008).

(Z)-4-methyl-5-[2-(3-(tifluoromethyl)phenyl)hydrazono]-2,6-dioxo-1-phenyl-1,2,5,6-tetrahydro-3-carbonitriles (**9**, $C_{20}H_{13}N_4O_2F3$).

Yellow-orange powder; yield 76%, m.p.: 259–61 °C.

^{1}H NMR (500 MHz, DMSO-d_6): δ = 2.63 (s, 3H, 4-CH_3), 7.26–7.33 (m, 2H, 2′-H, 6′-H), 7.45–7.53 (m, 3H, 3′-H, 4′-H, 5′-H), 7.61 (d, 1H, J = 7.5, 6″-H), 7.70 (t, 1H, J = 16, 5″-H), 8.02 (d, 1H, J = 8.5, 4″-H), 8.08 (s, 1H, 2″-H), 14.37 (s, 1H, N—H) ppm; ^{13}C NMR (125 MHz, DMSO-d_6): δ = 16.6 (C7), 101.7 (C3), 114.9 (C3″), 116.4 (C≡N), 120.9 (C4″) 122.7 (C2″), 122.5 (C5), 124.2 (CF_3), 128.7 (C4′), 128.8 (C3′, C5′), 128.9 (C2′, C6′), 131.6 (C6″), 134.0 (C1′), 137.5 (C5″), 142.8 (C1″), 159.6 (C2), 160.1 (C4), 160.4 (C6) ppm. IR (KBr): $\bar{\nu}$ = 685, 737, 778, 801, 838, 894, 954, 921, 955, 1002, 1033, 1097, 1123, 1156, 1223, 1278, 1329, 1405, 1465, 1489, 1509, 1581, 1640, 1693 (C═O), 2221 (C≡N), 3067, 3448 (O—H) cm^{-1}. Elemental Analysis:

Calculated: %C 60.30, %H 3.29, %N 14.07, %O 8.03, %F 14.31.

Found: %C 60.31, %H 3.27, %N 14.08, %O 8.01, %F 14.29.

(Z)-4-methyl-5-[2-(3-bromophenyl)hydrazono]-2,6-dioxo-1-phenyl-1,2,5,6-tetrahydro-3-carbonitriles (**10**, $C_{19}H_{13}N_4O_2Br$).

Orange powder; yield 66%, m.p.: 278–80 °C.

^{1}H NMR (500 MHz, DMSO-d_6): δ = 2.61 (s, 3H, 4-CH_3), 7.31–7.32 (m, 1H, 2′-H, 6′-H), 7.39–7.47 (m, 3H, 3′-H, 4′-H, 5′-H), 7.50–7.53 (m, 2H, 2″-H, 5″-H), 7.70–7.72 (m, 1H, 6″-H), 7.92–7.93 (m, 1H, 4″-H), 14.29 (s, 1H, N—H) ppm; ^{13}C NMR (125 MHz, DMSO-d_6): δ = 16.6 (C7), 101.7 (C3), 114.9 (C2″), 116.4 (C≡N), 119.9 (C6″), 122.5 (C5), 124.2 (C4″), 128.7 (C4′), 128.8 (C3′, C5′), 128.9 (C2′, C6′), 129.1 (C3″), 131.6 (C5″), 134.6 (C1′), 142.8 (C1″), 159.6 (C2), 160.1 (C4), 160.4 (C6) ppm. IR (KBr): $\bar{\nu}$ = 677, 689, 743, 777, 835, 870, 895, 954, 993, 1034, 1065, 1095, 1155, 1208, 1276, 1303, 1330, 1404, 1426, 1511, 1578, 1638, 1689 (C═O), 2222 (C≡N), 3073, 3451 (O—H) cm^{-1}.

Elemental Analysis:

Calculated: %C 55.76, %H 3.20, %N 13.69, %O 7.82, %Br 19.53.

Found: %C 55.75, %H 3.22, %N 13.70, %O 7.80, %Br 19.52.

(Z)-4-methyl-5-[2-(3-clorophenyl)hydrazono]-2,6-dioxo-1-phenyl-1,2,5,6-tetrahydro-3-carbonitriles (**11**, $C_{19}H_{13}N_4O_2Cl$).

Brownish-red powder; yield 72%, m.p.: 235–7 °C.

^{1}H NMR (500 MHz, DMSO-d_6): δ = 2.60 (s, 3H, 4-CH_3), 7.29–7.32 (m, 2H, 2′-H, 6′-H), 7.45–7.52 (m, 3H, 3′-H, 4′-H, 5′-H), 7.63–7.66 (m, 1H, 6″-H), 7.84–7.87 (m, 1H, 5″-H), 8.00 (d, 1H, J = 7, 4″-H), 8.07 (s, 1H, 2″-H), 14.28 (s, 1H, N—H) ppm; ^{13}C NMR (125 MHz, DMSO-d_6): δ = 16.6 (C7), 101.8 (C3), 114.9 (C2″), 116.9 (C≡N), 117.0 (C6″), 124.1 (C5), 126.2 (C4″), 128.7 (C4′), 128.8 (C3′, C5′), 128.9 (C2′, C6′), 131.3 (C1′), 133.9 (C5″), 134.2 (C3″), 142.7 (C1″), 159.6 (C2), 160.0 (C4), 160.4 (C6) ppm. IR (KBr): $\bar{\nu}$ = 676, 691, 704, 745, 784, 836, 868, 955, 996, 1033, 1071, 1095, 1156, 1211, 1283, 1332, 1405, 1432, 1455 1509, 1581, 1642, 1690 (C═O), 2221 (C≡N), 2851, 2922, 3073, 3443 (O—H) cm^{-1}. Elemental Analysis:

Calculated: %C 62.56, %H 3.59, %N 15.36, %O 9.77, %Cl 9.72.

Found: %C 62.55, %H 3.57, %N 15.37, %O 9.79, %Cl 9.74.

2.3. Ab initio theoretical calculation method

The geometry optimizations for compounds **1–6** and **8–11** were carried out in *N*-methylformamide using ωB97X-D functional (Chai and Head-Gordon, 2008) and standard basis set, 6-311G (d,p). Compound **7** (with I substituent) was excluded from theoretical considerations since basis set for iodine atom was not available. The solvation effect was simulated with standard polarized continuum model (PCM) (Tomasi et al., 2005). For all optimized structures harmonic vibrational frequencies were evaluated at the same level to confirm the nature of the stationary points found (to confirm that optimized geometry corresponds to local minimum that has only real frequencies), and to account for the zero point vibrational energy (ZPVE) correction. Global minima were found for every isomer considering **Hydrazo**, **Azo/a** and **Azo/b** tautomeric forms of obtained dyes, and rotational isomers of *meta*-substituted derivatives. Solvation free energies were calculated on PCM/ωB97X-D/6-311G(d,p) optimized geometries with SMD method (Marenich et al., 2009) in NMF solution, using the same functional and basis set. NMR chemical shifts are calculated on ωB97X-D/6-311G(d,p) optimized structures using GIAO approximation in Dimethyl sulfoxide (DMSO) as a solvent, with the specially parameterized WP04 functional and cc-pVDZ basis set. This method was proven to give best accuracy/cost ratio in NMR chemical shift prediction (Jain et al., 2009). The values of ^{1}H and ^{13}C chemical shifts presented in Table S2 are scaled relative to ^{1}H and ^{13}C chemical shift of TMS, and calculated with the same method. Atom numbering used in NMR calculations and assignment of chemical shifts are given in Fig. S1. All quantum chemical calculations were done with Gaussian09 program package (Frisch et al., 2009). Atoms in molecule (AIM) topological analysis was conducted with Multifwfn (version 3.3.7) program package (Lu and Chen, 2012). AIM analysis, Molecular electrostatic potential (MEP) maps and molecular orbital analysis were done on geometries and wave functions obtained from PCM/ωB97X-D/6-311G(d,p) calculations in NMF solution. Plot of Noncovalent interaction index (NCI) was done with NCIPLOT program (Johnson et al., 2010).

3. Results and discussion

3.1. Synthesis and stability of arylazo pyridone dyes

It was shown that synthesized pyridones, tautomeric mixture of 6(2)-hydroxy-4-methyl-2(6)-oxo-1-phenyl-1,2(1,6)-dihydro pyridine-3-carbonitriles – pyridone **a** and **b**, respectively, offered an interesting synthetic alternative: diazotization of pyridones gave only one product (*Z*)-6-hydroxy-4-methyl-5-[2-(4-nitrophenyl)hydrazono]-2,6-dioxo-1-phenyl-1,2,5,6-tetrahydro-3-carbonitrile (Ajaj et al., 2013). Spectral assignments of NMR data undoubtedly confirmed presence of (*Z*)-6-hydroxy-4-methyl-5-[2-(4-nitrophenyl)hydrazono]-2,6-dioxo-1-phenyl-1,2,5,6-tetrahydro-3-carbonitrile and non-reacted pyridone in ^{1}H NMR spectrum of unpurified product (Ajaj et al., 2013). DFT calculations confirmed higher stability of **Hydrazo** form due to formation of intra-molecular hydrogen bond (Fig. 1). It was assumed that equilibrium is shifted from **Azo** derivatives to more stable **Hydrazo** form *via* the most probable H-transfer from O(6)—H through pseudo-cyclic six-membered transition state *via* **Azo**/**a** form (Fig. 1). Two probable reaction pathways could lead to **Hydrazo** form: diazotization of pyridone **b** to **Azo**/**b** (path **i**) and consecutive transformation to **Azo**/**a** or by equilibrium shifts from pyridone **b** to **a** form followed by diazotization (path **ii**) (Fig. 1). The electrophilic displacement of hydrogen at C5 carbon of pyridone core is caused by substituent present in diazonium salt and the value of charge density at C5 carbon. The higher negative charges at C5 of tautomer **a**, obtained by DFT calculation (Ajaj et al., 2013), indicated higher probability that reaction takes *via* tautomer **a**. The optimized geometry of pyridone indicates *co*-planarity of electron-donating hydroxyl group at C6 in **a** form and π-electrons density of the C5—C6 double bond which provides higher extent of electron density shift to C5 carbon (*n*,π-conjugation). The consequence is more favorable reaction pathway (**ii**). Due to that, it was valuable to study **Azo**–**Hydrazo** tautomerism of synthesized azo pyridone dyes.

3.2. Spectral characteristics and tautomerism of arylazo pyridone dyes

The synthesized arylazo pyridone dyes exist as an equilibrium of two **Azo** forms, **Azo**/**a** and **Azo**/**b**, obtained by direct diazotization of tautomeric pyridones (Fig. 1), or by hydrogen transfer leading to more stable **Hydrazo** form. Predominance of **Hydrazo** form in a product has been confirmed by the data obtained from NMR analysis and quantum chemical calculations (Ajaj et al., 2013). Higher stability of **Hydrazo** form is confirmed by experimental and theoretical results obtained in this work. Examples of FTIR (Fig. S2), ^{1}H NMR (Fig. S3) and ^{13}C NMR (Fig. S4) spectra of compounds **1**, **4** and **5** are given in Supplementary material. DFT calculation of NMR chemical shift, obtained on ωB97X-D/6-311G(d,p) optimized geometries by using GIAO/WP04/cc-pVDZ method (Table S2; comps. **1** and **4**), proved accuracy of NMR data assignment and dominance of **Hydrazo** form. This is a powerful method used for prediction and interpretation of the structure and **Azo**/**Hydrazo** tautomeric equilibria in DMSO. The calculations in DMSO have also shown that energies of **Azo/a** tautomers are 107–111 kJ/mol higher and **Azo/b** tautomers are the least stable (in the range 116–120 kJ mol^{-1}) comparing to **Hydrazo** form. Detailed analysis on stability of all forms in NMF is given in Section 3.6.

The infrared spectra of all synthesized dyes showed two intense carbonyl bands at ≈1640 and ≈1690 cm^{-1}, which were assigned to 2,6-diketo groups present in **Hydrazo** form. Additionally, in some spectra observed bands in the region 3037–3125 cm^{-1} and 3431–3448 cm^{-1} were assigned to the N—H group from **Hydrazo** form and hydroxyl group in pyridone ring, respectively (Fig. S2). The ^{1}H NMR spectra of dyes showed a broad signal in the range of 14.26–14.69 ppm (Fig. S3), which corresponds to amino proton positioned in de-shielding region of phenyl group of the **Hydrazo** form (Fig. 1). The assumption is that substituent electronic effect does not cause significant influence on secondary magnetic field and, thus, it is reflected in lower effect on NMR shift change. Similar results were obtained for ten 5-arylazo-6-hydroxy-4-methyl-3-cyano-2-pyridone dyes that exhibit existence only of the **Hydrazo** tautomeric form in solid state and in solvent DMSO-d_6, with N—H ^{1}H NMR peak in the range of 14.35–14.87 ppm (Uščumlić et al., 2004). It was also shown that peak shift in ^{1}H NMR spectra is a consequence of appropriate solvent influence on the presence of predominating tautomeric **Hydrazo** form of **Azo** pyridone dyes in CF_3COOD/$CDCl_3$ solvent mixture, with N—H signal position shifting to higher value in the range 15.1–15.6 ppm (Ertan and Gurkan, 1997). The ^{13}C NMR studies of some *N*-alkyl derivatives of azo pyridones in $CDCl_3$ and DMSO-d_6 undoubtedly confirmed the presence of the **Hydrazo** form (Lučka and Machaček, 1986; Cee et al., 1988). Due to the importance of arylazo dyes, a detail analysis of the solvent and substituent effect on the state of tautomeric equilibria shift in synthesized dyes was conducted. Moreover, the analysis of the substituent effect on NMR chemical shifts, together with quantum chemical calculation, gave a range of valuable results that support presented conclusions.

A variety of spectroscopic methods could be used for analysis of the state of tautomeric equilibria, *i.e.* study of the mechanism of tautomer transformation. Exceptionally, at slow proton exchange, observation of a distinct signals in ^{1}H NMR spectra allows quantitative determination of tautomeric forms (Ajaj et al., 2013; Kolehmainen et al., 2000; Manolova et al., 2014; Ortiz et al., 2014). NMR analysis of the spectra of arylazo pyridone dyes did not allow determination of tautomers due to fast proton exchange at timescale (Figs. S3 and S4). Due to this, the study of the tautomeric equilibria is based on advantageous characteristics of UV–Vis spectroscopy: diversity of spectral properties of the corresponding tautomers, sensitivity of the tautomeric equilibria to the effect of surrounding solvent (environment), solvent basicity and acidity, substituent effect present at solute molecule, as well as operational temperature. An algorithm consisted in stepwise methodology (Antonov and Stoyanov, 1993; Antonov, 2013) was used for the resolution of the UV–Vis spectra of arylazo pyridone dyes studied in this work. Absorption spectra of the arylazo pyridone dyes **1**–**11**, recorded in seventeen solvents, indicate the presence of the overlapped bands in the region 350–500 nm (Fig. 2). All UV–Vis spectra were recorded at concentration of 1×10^{-5} mol dm^{-3}, and mean values from three measurements were presented.

Dimerization process, which is favorable for 2-pyridone at higher concentrations (Szyc et al., 2010), was not usually found for solute concentration lower than 1×10^{-5} mol dm^{-3}. Strong tendency of 2-pyridone to create intermolecular hydrogen-bridged dimer was the process of negligible contribution to the previously studied tautomeric *N*(1)-substituted pyridones. Low extent of dimerization in arylazo pyridone dyes is a consequence of low degree of lateral π,π-stacking interaction due to deflection of the *N*(1)-phenyl ring, and the similar was found for pyridone precursor (Ajaj et al., 2013). Two additional factors contribute to absence of dimerization: the introduction of 5-arylazo group at pyridone core contribute to structure crowdness and adverse/higher intensity of solvent/solute interactions, with respect to attractive interactions among molecules. The characteristic absorption spectra of investigated compounds in NMF and DMF are shown in Fig. 2.

From the presented UV–Vis spectra (Fig. 2), diversity of the spectra could be noticed: wide to narrow shape, but all of them show large overlapping of the absorption bands which corresponds to appropriate tautomeric form. Successfulness of the methodology, applied for resolution of UV–Vis spectra, was necessarily based on appropriate approximations described in a previous work (Ajaj et al., 2013). Regardless of such limitations, it is widely used in scientific literature (Tsuno et al., 1975). A semi-quantitative approach gives satisfactory results related to the evaluation of the state of tautomeric equilibria (Antonov and Stoyanov, 1993, 1995; Petrov et al., 2000). The obtained spectra were analyzed by stepwise procedure: firstly, performing an estimation of tautomerization constants, individual spectra of the tautomers and absorption band numbers based on the results both experimental data and DFT calculation. The second and fourth derivative spectroscopy was helpful in determining the number and approximate position of the absorption bands corresponding to appropriate tautomeric form (Ajaj et al., 2014; Petrov et al., 2000). Afterward, an approximation of the band intensities and band widths, as well as the assignment to the appropriate tautomeric form was performed. The final refinement is performed by simultaneous resolution of the whole set of spectra according to the literature procedures (Ajaj et al., 2014;

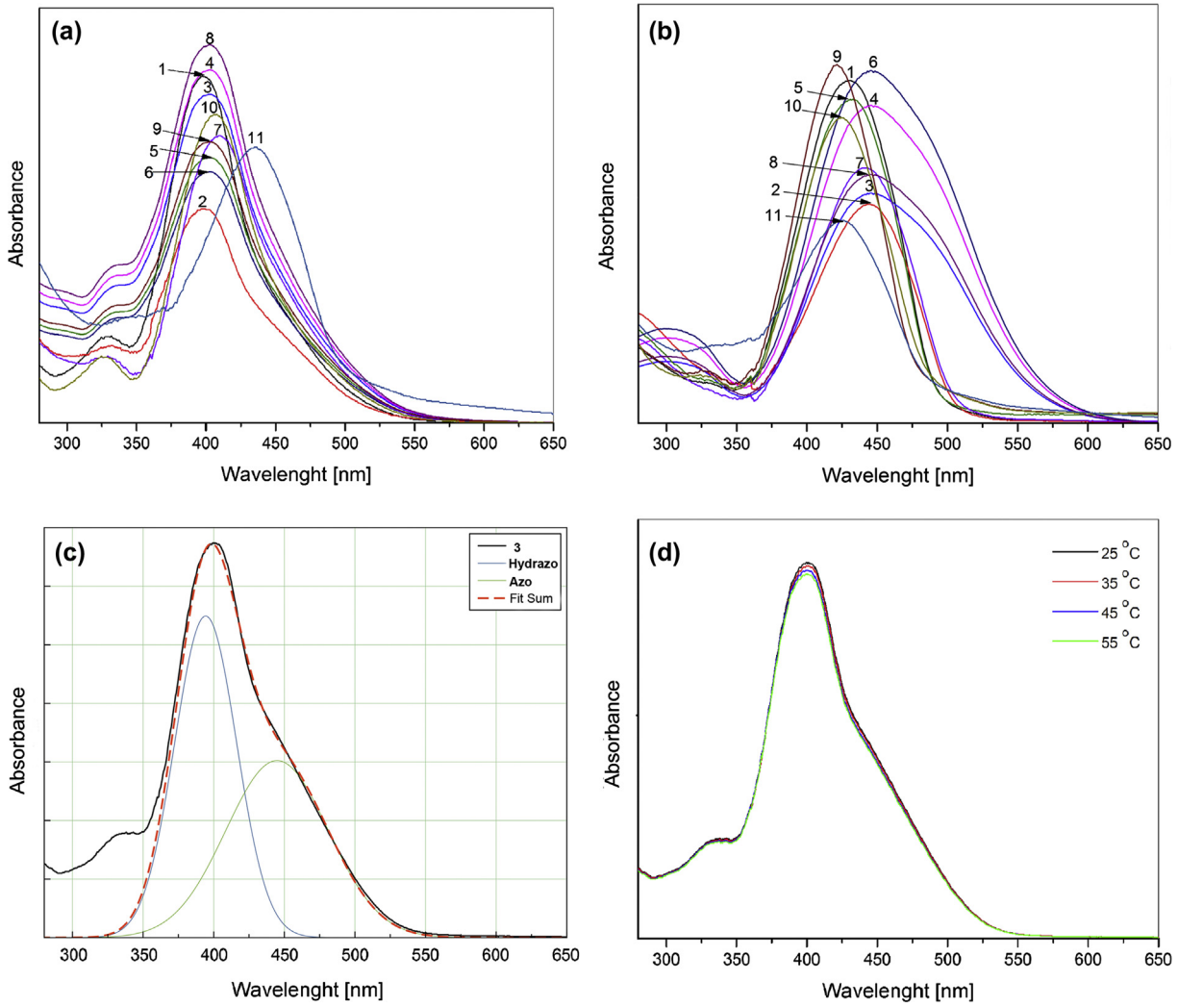

Figure 2 UV–Vis absorption spectra of compounds **1**–**11** in (a) NMF and (b) DMF, (c) resolved overlapping bands of compound **3** in NMF, and (d) temperature-dependent spectra of compound **3** in NMF.

Antonov and Stoyanov, 1993, 1995; Antonov, 2013). The results of the applied methodology are exemplified in Fig. 2c, and absorption maxima of both **Hydrazo** (lower wavelength band) and **Azo/a** form (higher one) obtained in the set of selected solvents are summarized in Tables 2 and 3, respectively. Low temperature influence on absorption spectra change was found (example given for compound **3** in Fig 2d), and additionally confirmed that negligible extent of dimerization exists in solution.

The data from Table 2 indicate that values of absorption frequencies of investigated compounds depend on the substituent effect. The introduction of *methoxy*, *nitro*, *bromo* and *iodo* substituents contributes to the positive solvatochromism, comparing to the unsubstituted compound, while the other compounds show shifting to lower wavelength. The absorption spectra showed relatively low dependence on both solvent and substituent effects, *i.e.*, the absorption bands of both electron-donor and electron-acceptor substituted derivatives appear at similar wavelengths (in the range 10–20 nm) compared to parent compound **1**.

Applying described methodology given in previous publication (Ajaj et al., 2013), K_T values, K_T = [**Hydrazo**]/[**Azo/a**], of the investigated compounds were determined in DMF, DMAc and NMF, and the results are presented in Table 4. The changes in the K_T values are consequence of the balanced contribution of both solvent and substituent effects. The NMF solvent effect on K_T change (contribution of both dipolarity/polarizability effect and hydrogen bonding ability) causes shift of the tautomeric equilibria to **Hydrazo** form (higher K_T values). The highest value of K_T was found for halogen substituted azo dyes. The opposite is true for aprotic solvents DMF and DMAc, *i.e.* solvent with increased dipolarity/polarizability causes complex influence on K_T values. It could be postulated that such a behavior is a consequence of different conjugational ability of the π-electron densities through localized or delocalized π-electronic systems of the appropriate tautomeric forms.

3.3. Solvent effects on the UV–Vis absorption spectra: correlation with multi-parameter solvent polarity scales

The UV–Vis spectra of arylazo pyridone dyes consisted of two strongly overlapped bands corresponding to **Hydrazo** form (lower one), and higher wavelength band ascribed to **Azo/a**

Table 2 Absorption maxima of the hydrazo (**Hydrazo**) form of investigated compounds in selected solvents.

Solvent/compound	$\nu_{max} \times 10^{-3}$ (cm^{-1})										
	1	**2**	**3**	**4**	**5**	**6**	**7**	**8**	**9**	**10**	**11**
Methanol	23.33	23.26	22.09	23.17	23.81	22.46	22.75	23.64	23.84	23.53	23.95
Ethanol	23.08	22.36	21.51	23.02	23.08	21.83	21.98	22.92	23.69	23.41	23.41
1-Propanol	23.01	22.24	21.39	22.96	23.01	21.62	21.51	22.84	23.39	23.34	23.24
2-Propanol	23.03	22.21	21.35	22.73	23.00	21.41	21.53	22.86	23.37	23.28	23.18
1-Butanol	22.94	22.19	21.28	22.86	22.97	21.36	21.46	22.81	23.31	23.24	23.06
2-Butanol	22.93	22.21	21.31	22.79	22.92	21.35	21.51	21.76	23.26	23.20	23.05
1,4-Dioxane (dioxane)	22.78	22.59	20.71	23.45	23.09	22.72	22.58	22.67	23.39	23.12	22.49
Ethyl acetate (EtAc)	23.31	22.86	21.91	23.21	23.51	22.35	22.46	23.72	23.46	23.54	23.61
Tetrahydrofuran (THF)	23.22	22.78	21.81	23.24	23.25	22.84	22.79	23.13	23.73	23.48	23.24
Acetonitrile (AcN)	24.03	24.21	23.15	23.91	24.19	23.65	23.89	23.17	23.84	24.03	23.58
Acetone	23.29	22.71	22.54	23.51	23.26	22.76	22.81	23.12	23.81	23.43	23.87
Dimethyl sulfoxide (DMSO)	24.82	24.89	24.83	22.45	24.91	24.37	24.36	24.75	24.25	24.26	24.31
N,*N*-Dimethylformamide (DMF)	24.74	24.85	24.76	22.54	24.81	24.18	24.20	24.31	24.19	24.18	24.17
N,*N*-Dimethylacetamide (DMAc)	24.91	24.34	24.86	22.43	24.53	24.03	24.01	24.52	24.26	24.23	24.23
N-Methylformamide (NMF)	25.41	25.41	25.40	22.85	25.34	24.78	24.86	25.24	24.9	24.95	24.75
Dichloromethane (DCM)	25.19	25.23	25.39	24.87	25.23	24.98	24.99	25.35	25.39	25.01	25.31
Chloroform (Chl)	24.43	23.95	24.12	24.98	24.23	24.31	24.23	24.21	24.76	24.36	24.45

Table 3 Absorption maxima of **Azo/a** form found in selected solvents.

Solvent/compound	$\nu_{max} \times 10^{-3}$ (cm^{-1})										
	1	**2**	**3**	**4**	**5**	**6**	**7**	**8**	**9**	**10**	**11**
THF	–	–	–	22.31	–	–	–	–	–	–	–
AcN	–	–	–	22.55	–	–	–	22.17	–	–	22.43
DMSO	–	–	–	19.31	–	–	–	–	–	–	–
DMF	22.79	22.82	21.97	19.99	22.61	22.13	22.18	22.44	–	–	20.37
DMAc	22.83	22.67	22.21	19.93	22.58	22.07	22.23	22.47	–	–	20.41
NMF	22.48	21.86	22.4	20.14	23.31	22.02	22.15	22.25	–	–	21.04

Table 4 Equilibrium constants K_T of the investigated arylazo dyes at 25 °C.

Solvent/compound	K_T = **Hydrazo/Azo**										
	1	**2**	**3**	**4**	**5**	**6**	**7**	**8**	**9**	**10**	**11**
THF	–	–	–	2.22	–	–	–	–	–	–	–
AcN	–	–	–	2.05	–	–	–	0.55	–	–	0.47
DMSO	–	–	–	0.73	–	–	–	–	–	–	–
DMF	1.11	1.05	0.87	0.19	1.20	1.96	2.13	1.60	1.26	1.35	1.42
DMAc	1.34	1.02	0.91	0.52	1.35	2.15	1.98	1.73	1.26	1.43	1.40
NMF	1.69	1.39	1.18	1.04	1.56	2.02	2.15	2.02	1.33	1.53	1.44

form. The absorption maxima, corresponding to electron density transition from the **Hydrazo** NH group to the pyridone carbonyl groups (lower energy band) in investigated dyes, are presented in Table 2. The absorption maxima, which correspond to presence of **Azo/a** form, are given in Table 3. The data from Tables 2 and 3 confirm that the positions of the UV–Vis absorption frequencies depend on the nature of the solvent used and substituent. The introduction of electron-donating or electron-attracting substituents in the phenyl ring in all solvents causes variation of the bathochromic or hypsochromic shifts compared to that of the comp. **1**.

The effect of solvent dipolarity/polarizability and hydrogen bonding ability on the absorption maxima shift were interpreted by applying principles of linear solvation energy relationship (LSER) using a Kamlet–Taft solvatochromic Eq. (1) (Kamlet et al., 1981). The correlations of the absorption frequencies maxima ν_{max} for **Hydrazo** tautomer were carried out by means of multiple linear regression analysis. The results are presented in Table S3, and coefficients ν_0, s, b and a fit at the 95% confidence level.

The non-specific solvent effect is a factor of the highest contribution to UV–Vis spectral shifts of all investigated com-

pounds (Table S3). According to the correlation results, the negative sign of *b* coefficient, for all arylazo pyridone dyes (Table S3), indicates a bathochromic shift with increasing solvent hydrogen-bond accepting capability. This suggests better stabilization of the electronic excited state relative to the ground state. The positive sign of *s* and *a* coefficients for all investigated dyes indicates hypsochromic shifts with increasing solvent dipolarity/polarizability and hydrogen-bond donor capability. This suggests better stabilization of the ground state relative to the electronic excited state with increasing solvent polarity, *i.e.* higher dipolar properties of molecule in the ground state. The percentage contribution of solvatochromic parameters (Table S3) for all azo dyes showed that the most of the solvatochromism is due to solvent dipolarity/polarizability rather than the solvent hydrogen-bonding ability. Presented results, obtained by the use Kamlet–Taft model, indicate that the solvent effects on azo–hydrazo tautomeric equilibrium and UV–Vis spectra are very complex due to diversity of the contribution of both solvent and substituent effect in studied azo dyes. This also indicated that the electronic behavior of the nitrogen atoms of hydrazo group is different between derivatives with electron-donating and electron-accepting substituents.

In order to investigate the influence of the substituent electronic effects to the state of tautomeric equilibria, $\log K_T$ values were correlated with combination of substituent constants, σ_p/σ_m and σ_p^+/σ_m^+ (Table S4), and the results obtained for DMF, DMAc and NMF are presented in Table S5. The results of correlation analysis of the substituent effect on tautomeric equilibria pointed out that there are two different trends involving two groups of substituents (Table S5). The first group, that includes electron-donating substituents and *chloro* substituent, exhibits similar sensitivity of $\log K_T$ to substituent effect, irrespective of solvent used. Similar correlation coefficients and lower ρ values were obtained by using electrophilic substituent constants. These results indicate low contribution of extended resonance interaction through overall molecule. In that way, stable intramolecular hydrogen bonding bridge N2—H···O=C6 is established, causing stabilization of pseudo six-membered heterocyclic ring, and consequently, higher planarization of the molecule as a whole (Fig. S5; structure a). Due to overall planarization, transmission of electronic substituent effects exhibits low sensitivity to external factors such as solvent effects. The second group of substituents contains compounds with electron-accepting substituents and *halogen* substituted ones. The negative sign of proportionality constant, ρ, for second series means reverse behavior, *i.e.* it indicates equilibrium shift to **Azo/a** form with increasing electron-accepting character of the substituent. The most pronounced sensitivity to solvent effects, in second series, was found for DMF, lower for DMAc (it displays lower proton-accepting capability), and the lowest for NMF solvent due to obvious proton-donating effect of N—H hydrogen. Higher sensitivities of $\log K_T$ to substituent effects in solvent with higher relative permittivity can be explained by the fact that, in dipolar surrounding medium, energies necessary to bring about charge separation in the ground and excited state are relatively similar inducing higher susceptibility of $\log K_T$ to electronic substituent effects. Tautomeric equilibrium shift to **Azo**/**a** form is a consequence of electronic density shift in electron-acceptor substituted **Hydrazo** form (Fig. S6; structure f) favoring hydrogen transfer to C6 carbonyl oxygen.

3.4. Substituent effects on the NMR data: LFER analysis

The LFER concept was applied to the *SCS* values of arylazo pyridone dyes with the aim to get an insight into substituent electronic effect to the absorption maxima shifts and NMR chemical shifts. A correlation analysis, by using LFER principles, in the form of the Hammett equation was performed (Hammett, 1937), and obtained results are given in Tables S6 and S7.

The observed ρ values indicate different susceptibilities of the *SCS* to substituent effects. It can be noticed from Table S6 that correlations are of good to high quality which means that the *SCS* values reflect electronic substituent effects. It is apparent that chemical shifts of C5 show an increased susceptibility and normal substituent effect. Reverse substituent effect was observed for C2, C3, C4 and C6 carbons. The existence of these correlations was interpreted as an evidence of substituent effect on the state of azo–hydrazo tautomerism. The azo group (—N=N—) is an electron-accepting group, while the imino group (—NH—) present in **Hydrazo** form is an electron-donating group. According to that, it is expected that electron-accepting group stabilizes the **Hydrazo** form. Presented results indicate that both substituents, electron-donating and electron-accepting, have significant influence on stabilization of **Hydrazo** tautomeric form. Detail analysis of the transmission substituent effect through resonance structures of investigated arylazo pyridone dyes is presented on pages 15–16 in Supplementary material.

Contributions of the polar and resonance effects of substituents were performed by using DSP Eq. (3) with σ_I and σ_R constants, and the results are given in Table S7. The effectiveness of the transmission of substituent effects is determined, among other factors, by the conformational (geometry) change of the investigated molecules which stems from an out-of-plane rotation of the *N*(1)-phenyl and arylazo rings, defined by the torsion angles θ_1 and θ_2, respectively (Fig. 1). The results obtained by the use of DSP equation do not provide significant improvement in fits when compared to the results obtained by the use of SSP Eq. (2). However, on the other hand, DSP results are useful for the estimation of contribution of appropriate substituent effects on *SCS* change of the atom of interest. It is obvious that chemical shifts of C5 show an increased susceptibility and normal substituent effect. Reverse substituent effect was observed at C2, C3, C4 and C6 carbons (Table S6). The negative sign of reaction constant, ρ, indicates reverse behavior, *i.e.* the value of *SCS* decreases although the electron-withdrawing ability of the substituents, measured by σ, increases.

Correlations for C5 carbon give λ ($=\rho_R/\rho_I$) value of 1.3 which means that higher contribution of resonance interaction with electron density at this carbon is operative through hydrazo group. Conformational arrangement of the phenyl hydrazo moiety, due to formation hydrogen bridged six membered structures, provides effective transmission of the extended resonance effect to C5 carbon. All other λ values are lower than 1, which means that polar (inductive/filed) substituent effect predominates over resonance effect. The alternation of polar substituent effects has been manifested as

variation of the values of ρ_I coefficients (Table S6) which reflect distance/angle dependence of field effect as well as path-length dependence of the inductive substituent effect.

3.5. Substituent effects on the UV data: LFER analysis

The correlation results of UV–Vis absorption maxima for arylazo pyridone dyes, obtained by the use of principles of LFER analysis, are given in Table 5. The LFER results indicate complex influences of both solvent and substituent effect on UV–Vis absorption maxima of **Hydrazo** form (Table 5). These results also indicate that solvent effects: dipolarity/polarizability, HBD and HBA abilities cause appropriate sensitivity of the position of absorption maxima (ν_{max}) to substituent effect.

Generally, the correlation results could be divided into two sets: the first set includes protic solvents (alcohols), THF, acetone, Chl and EtAc with positive correlation coefficients. Higher susceptibility of the ν_{max} shifts to the electronic substituent effects was found for these set of solvents, and the highest influence was found in EtAc. The hydrogen-bonding ability of protic solvent is the factor of primary significance which contributes to better stabilization of the ground state. Somewhat lower negative values of correlation coefficients were found for other solvents (second set), indicating the significance of solvent dipolarity/polarizability effect to better stabilization of excited state. Highly dipolar aprotic solvents contribute to the lower sensitivities of absorption frequencies to substituent effects. Aprotic solvents behave as poor anion solvators, while they usually better stabilize larger and more dispersible positive charges. Lower contribution of substituent effects in solvent with higher relative permittivity can be explained by the fact that highly dipolar surrounding medium suppresses electron density shift inducing lower susceptibility of absorption maxima shift to electronic substituent effects.

Presented results showed that transmission of substituent electronic effects through π-resonance units takes place by balanced contribution of two modes: through localized π-electronic unit and overall conjugated system of arylazo pyridone dyes. Their contribution depends on substitution pattern, as well as solvent under consideration. It was found that extended resonance interaction is effectively transmitted to C5 carbon showing normal substituent effect (Table S7), which confirms that pseudo-cyclic hydrogen bridge plays significant role in transmission of substituent effects. Mode and range of the transmission of substituent effect is provided in Supplementary material (pages 14–16).

3.6. Results of DFT calculations. Nature of the frontier molecular orbitals

The geometries of all tautomers of investigated arylazo pyridone dyes were optimized in NMF solution with ωB97X-D/6-311G(d,p) method. The ωB97X-D functional was used because it includes empirical dispersion and long range corrections. Recent benchmark studies have shown a very good behavior of this functional for describing geometry and energy of strong hydrogen bonds (Thanthiriwatte et al., 2011). The calculations have shown that for all investigated compounds **Hydrazo** tautomer, with intra-molecular hydrogen bond, is the most stable tautomer. The energies of **Azo/a** tautomers

Table 5 Correlation results of the absorption maxima of compounds **1–11** in **Hydrazo** form with σ_p/σ_m and σ_p^+/σ_m^+ substituent constants.

Solvent	$\nu_0 \times 10^{-3}$ (cm^{-1})	$\rho \times 10^{-3}$ (cm^{-1})	R	Sd	F	$\nu_0 \times 10^{-3}$ (cm^{-1})	$\rho \times 10^{-3}$ (cm^{-1})	R	Sd	F	Substituents
	σ					σ^+					
Methanol	23.38 ± 0.10	1.31 ± 0.27	0.890	0.29	23	23.38 ± 0.11	1.24 ± 0.28	0.875	0.31	20	NO_2, Br, I excluded
Ethanol	22.62 ± 0.13	2.37 ± 0.46	0.901	0.32	26	21.88 ± 0.06	1.56 ± 0.16	0.971	0.18	97	
1-Propanol	22.52 ± 0.14	2.25 ± 0.49	0.882	0.34	21	22.75 ± 0.08	1.49 ± 0.19	0.955	0.22	63	
2-Propanol	22.50 ± 0.14	2.23 ± 0.51	0.871	0.36	19	22.73 ± 0.08	1.49 ± 0.20	0.948	0.23	53	
1-Butanol	22.44 ± 0.15	2.20 ± 0.52	0.865	0.37	18	22.67 ± 0.09	1.47 ± 0.21	0.943	0.24	48	
2-Butanol	22.45 ± 0.16	2.14 ± 0.55	0.867	0.38	15	22.66 ± 0.10	1.42 ± 0.22	0.945	0.25	42	NO_2, Br, I, Cl excluded
Dioxane	21.86 ± 0.20	2.66 ± 0.50	0.909	0.39	29	22.25 ± 0.11	1.77 ± 0.22	0.956	0.27	64	H, Me, F excluded
EtAc	23.16 ± 0.14	3.40 ± 0.78	0.930	0.31	19	23.48 ± 0.07	2.00 ± 0.20	0.986	0.14	103	H, Me, OMe, F, Cl
	23.91 ± 0.05	−0.92 ± 0.10	0.981	0.04	78	23.85 ± 0.05	−0.76 ± 0.10	0.973	0.05	52	Cl, 3-CF_3, 3-Br, 3-Cl, NO_2
AcN	24.07 ± 0.03	−1.28 ± 0.30	0.905	0.13	18	23.98 ± 0.05	−1.01 ± 0.06	0.907	0.13	19	H, Me, NO_2, F, Br, I
THF	22.84 ± 0.14	1.83 ± 0.48	0.840	0.34	14	23.03 ± 0.08	1.25 ± 0.19	0.934	0.22	41	NO_2, Br, I excluded
Acetone	23.05 ± 0.09	1.59 ± 0.31	0.902	0.22	26	23.22 ± 0.07	1.00 ± 0.17	0.927	0.19	37	
DMSO	24.83 ± 0.07	−1.22 ± 0.25	0.907	0.14	23	24.74 ± 0.05	−0.96 ± 0.15	0.945	0.11	41	NO_2, Br, I, OMe
DMF	24.71 ± 0.05	−1.33 ± 0.19	0.954	0.10	51	24.61 ± 0.06	−0.97 ± 0.18	0.925	0.13	30	excluded
DMAc	24.62 ± 0.04	−0.90 ± 0.11	0.970	0.07	64	24.49 ± 0.03	−0.50 ± 0.06	0.975	0.06	76	OMe, F, Cl, 3-CF_3, 3-Br, 3-Cl
	24.43 ± 0.22	−2.36 ± 0.58	0.921	0.42	17	24.25 ± 0.25	−2.01 ± 0.64	0.877	0.51	10	H, Me, Br, I, NO_2
NMF	25.35 ± 0.04	−0.92 ± 0.16	0.941	0.09	31	25.29 ± 0.04	−0.69 ± 0.12	0.946	0.08	34	H, Me, OMe, F, Br, I
	25.32 ± 0.09	−1.68 ± 0.21	0.939	0.26	67						All (NO_2 (σ^-))
DCM	25.18 ± 0.03	−0.48 ± 0.09	0.909	0.08	29	25.13 ± 0.02	−0.35 ± 0.06	0.932	0.07	40	Cl, 3-CF_3, 3-Cl excluded
Chl	24.08 ± 0.06	1.10 ± 0.16	0.936	0.12	49	24.18 ± 0.05	0.89 ± 0.12	0.942	0.11	55	Cl, 3-CF_3, 3-Cl excluded

are from 93.55 to 97.68 kJ/mol higher than **Hydrazo** form, while the **Azo/b** tautomers are the least stable (Table 6). The large energy differences between tautomers indicate that an intra-molecular hydrogen bond formed in **Hydrazo** tautomer is very strong in nature. This was further confirmed by structural and topology analysis. The distances between oxygen and hydrogen atoms involved in hydrogen bond creation in **Hydrazo** tautomers are from 1.869 to 1.883 Å (Table 6), which are much shorter than sum of their van der Waals radii (2.6 Å). AIM topological analysis has found a bond critical point (BCP) between oxygen and hydrogen atom in **Hydrazo** tautomer of every investigated compound. Data about found BCPs are summarized in Table 6. Values for total electronic density (ρ) at BCP (from 0.0326 to 0.0336; Table 6) fall at the high density range for hydrogen bond (0.002–0.035) (Koch and Popelier, 1995). Since total electron density at the BCP correlates with hydrogen bond strength (Koch and Popelier, 1995; Yuan et al., 2010) high electron density values in **Hydrazo** tautomers further confirm a presence of very strong hydrogen bond. Also, there is a good correlation between O···H distance values and electron densities and Laplacian of electron densities ($\nabla^2\rho$) for all **Hydrazo** tautomers (Table 6). Plot of Non-Covalent Interaction (NCI) index and position of BCP for compound **1** is shown in Fig. 3.

Values of solvation free energy dG_{solv}, calculated by SMD method, are presented in Table 6. For all compounds **Azo**/**a** tautomers have the highest and **Hydrazo** tautomer the lowest dG_{solv} values, but the difference is only between 11.51 and 17.25 kJ/mol, so the solvation effect does not have significant influence on the stability of tautomers. Interestingly, in NMF solvent, due to high value of dielectric constant and hydrogen bonding ability, the optimization of molecular structure of tautomer **Azo**/**a** was successful. Otherwise, in other solvents, as well as in gas phase, calculations have shown that **Azo**/**a** tautomer is not a minimum on potential energy surface. All DFT optimizations, which started from **Azo**/**a** geometry, are optimized to much more stable geometry of **Hydrazo** form. Theoretical calculations and NMR results clearly indicated that, if both tautomers (**Azo**/**a** and **Azo**/**b**) are obtained by pyridone diazotization (Fig. 1), subsequent hydrogen rearrangements drive the equilibrium to more stable **Hydrazo** form (Ajaj et al., 2013). It is additional evidence that **Hydrazo** form is the most stable molecular structure both in the gas phase and in solvated state. The optimized structures of **Azo**/**a**, **Azo**/**b** and **Hydrazo** forms of compounds **3** and **4** in NMF are shown in Fig. 4, and other compounds in Hydrazo form in Fig. S7. The elements of optimal geometry of arylazo pyridone dyes in **Hydrazo** form are presented in Table 7.

Table 6 Results of ωB97X-D/6-311G(d,p) and AIM calculations of investigated compounds.

Comp.	Tautomer	Energy (kJ/mol)	O···H (Å)	ρ	$\nabla^2\rho$	dG_{solv} (kJ/mol)	μ (D)
1	Azo/a	97.08				98.81	12.1679
	Azo/b	102.33				91.22	2.3635
	Hydrazo	0.00	1.883	0.0326	0.121	81.56	12.6971
2	Azo/a	95.79				97.84	12.6378
	Azo/b	100.86				92.97	1.4616
	Hydrazo	0.00	1.876	0.0331	0.123	82.51	13.6655
3	Azo/a	94.40				101.35	14.5098
	Azo/b	98.52				95.49	2.0283
	Hydrazo	0.00	1.869	0.0336	0.124	87.20	15.3977
4	Azo/a	97.68				96.59	9.6369
	Azo/b	105.03				90.50	10.0304
	Hydrazo	0.00	1.879	0.0328	0.123	85.92	6.0382
5	Azo/a	93.55				94.07	11.0185
	Azo/b	98.96				88.76	4.3028
	Hydrazo	0.00	1.878	0.0329	0.122	81.38	11.0186
6	Azo/a	95.79				99.19	10.5958
	Azo/b	101.54				94.28	5.1227
	Hydrazo	0.00	1.872	0.0333	0.124	87.13	10.1534
8	Azo/a	95.00				97.94	10.5355
	Azo/b	100.70				92.63	5.3040
	Hydrazo	0.00	1.876	0.0331	0.123	85.68	9.9863
9	Azo/a	95.42				93.69	10.2066
	Azo/b	101.93				88.08	6.6625
	Hydrazo	0.00	1.872	0.0333	0.124	82.18	9.4270
10	Azo/a	94.84				98.63	9.4884
	Azo/b	100.74				94.50	4.5371
	Hydrazo	0.00	1.875	0.0331	0.123	86.38	10.0990
11	Azo/a	94.65				97.36	9.2180
	Azo/b	101.25				92.37	4.7763
	Hydrazo	0.00	1.875	0.0331	0.123	84.73	9.9085

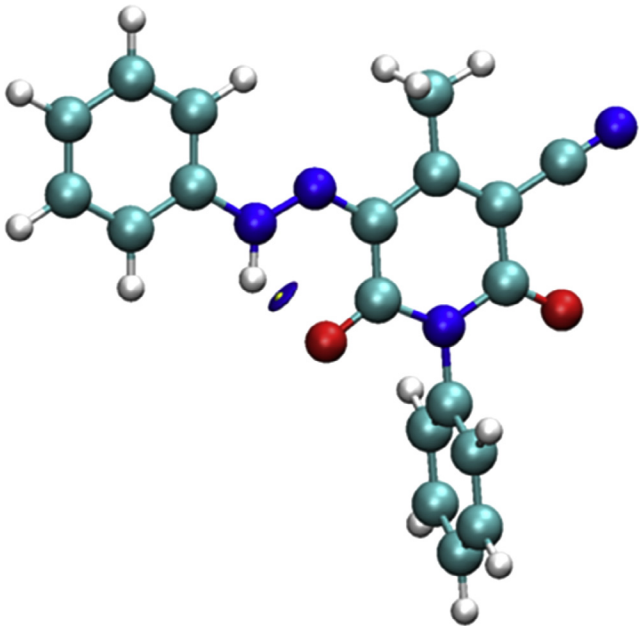

Figure 3 Plot of NCI index (blue surface) of **Hydrazo** tautomer of compound **1**. BCP of hydrogen bond is presented as yellow sphere. Blue color of NCI index indicates strong and attractive non-covalent interactions (Johnson et al., 2010).

The geometry parameters of the of substituted derivatives are similar to those for the unsubstituted one. The introduction of both electron-donor and electron-accepting substituents causes decrease of O···H hydrogen bond length (Table 6). An electron-donor substituent supports electron density shift from the phenylazo group to the pyridone moiety causing whole molecule planarization. An increase of the C5—N1 and decrease of N1—N2H bond lengths, which are part of the hydrazo group, contribute to a greater extent of the π,π-delocalization with π-electronic system of pyridone ring. As a consequence, the lengths of carbonyl groups are slightly longer in the electron-donor substituted derivatives. This result is an additional support for the extended conjugation, *i.e.*, the π-electron density shifts toward C6═O carbonyl group increasing both carbonyl bond lengths and supporting more intensive N2—H···O═C6 hydrogen bonding, *i.e.* interaction between keto-hydrazo groups in **Hydrazo** form (Fig. 1).

The results of geometry optimization are slightly different for the electron-acceptor substituted compounds. The low deviation from the planarity and an increase of the N1—N2H bond length and decrease of C5—N1 and N2—H bond lengths indicate that two opposite electron accepting effects operate in investigated compounds: electron-accepting phenylazo group and pyridone core cause appropriate geometrical adjustment as a response to electronic demand of the electron deficient environment (Fig. S6). The normal carbonyl groups polarization is suppressed and that causes a slight bond length decrease of carbonyl groups. More detail analysis of electronic structure of investigated dyes was presented on pages 14–17 in Supplementary material (Figs. S5 and S6). Electronic excitations and changes in the charge distribution, considering HOMO and LUMO orbitals, in both ground and excited states of the investigated molecules were studied by calculation of the energy gaps for all investigated compounds (Table 8), and results are presented in Figs. 5 and S12. The molecular orbitals and energy gaps between HOMO and LUMO orbitals, and MEP map of compounds **3** and **4** for all tautomers are given in Fig. 5.

The results indicate that HOMO of the neutral compounds is delocalized over the entire molecule, while LUMO is shifted toward the central pyridine and phenylazo rings. Furthermore, the ICT character could not be clearly observed during the orbital transition process from the HOMO to LUMO. The introduction of weak and moderate electron-donating *methyl* and *methoxy* group, respectively, in compounds **2** and **3,** produces appropriate change in the position of HOMO and LUMO orbital with respect to compound **1**. The energy gap between these compounds is lower than that for compound **1**, and the lowest value found for compound **3** because of the involvement of the electron-donating *methoxy* group, which brings about lower energy values of both HOMO and LUMO orbital. Due to more significant stabilization of LUMO orbital, slightly lower E_{gap} value was found for compound **3**. On the other hand, the introduction of the strong electron-withdrawing *nitro* group in compound **4** causes similar increase of energy for both HOMO and LUMO orbital which gives similar E_{gap} value as found for compound **1**. In addition, the introduction of the *nitro* group leads to a higher stabilization of both HOMO and LUMO orbitals. Halogen substituted compounds also do not produce any appreciable change of the position of HOMO and LUMO orbitals with respect to compound **1**. In compounds with *meta*-substituent **9**–**11**, both HOMO and LUMO orbitals are better stabilized than in other compounds (except for comp. **4)**, and E_{gap} values are higher than in other compounds due to significantly better stabilization of HOMO orbital (Table 8).

The variation of the substituent of different electron properties clearly indicates that contributions of both conformational arrangement and donor–accepting character are involved in the ICT mechanism of the investigated molecules.

Additionally, comprehensive correlation/inter-correlation of the experimental and calculated data with solvent and substituent parameters was performed. Correlation results of the absorption maxima of compounds **1**–**11** in **Hydrazo** form with calculated dipole moment values (μ) are given in Table S8 and Fig. S8. The correlation analysis of the dipole influences on the absorption maxima pointed out that there are three different trends involving three groups of solvents (Table S8). The first group includes alcohols and EtAc that exhibits general trend of bathochromic shift with increasing solvent polarity (Table S8 and Fig. S8a). The second group of solvents contains mostly strong dipolar aprotic solvents: DMF, DMAc, NMF, DMSO and DCM, which showed positive slope of correlation line. It means that higher electron-accepting substituents induce lower dipole moment of arylazo dyes, which is, therefore, more susceptible to interaction with dipolar aprotic solvent causing larger bathochromic shift (Fig. S8b). The third group of solvent, Chl and Dioxane, showed dual correlation lines: one, generally, mostly including strong electron-donating and electron-accepting substituents and the second one, the rest of the dyes. These correlations also indicate bathochromic absorption maxima shift with increasing solvent dipolar properties.

The correlation of the calculated E_{gap} values of compounds **1**–**11** of **Hydrazo** form in NMF solvent with Hammett σ_p substituent constants is given in Fig. S9, and correlation results by Eq. (S1). The correlation result indicates that both strong electron-donating and electron-accepting substituents cause

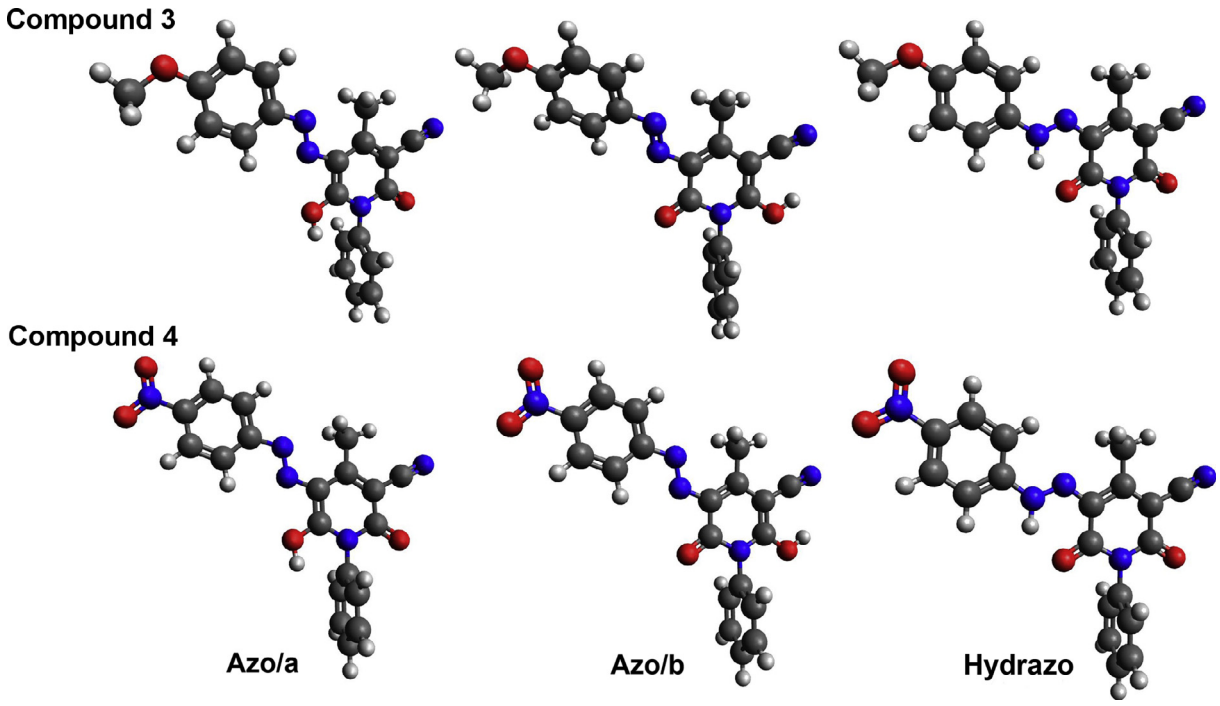

Figure 4 Optimal geometries of compounds **3** and **4** in the **Azo**/**a**, **Azo**/**b** and **Hydrazo** form in NMF obtained by ωB97X-D/6-311G(d,p) method Fig. 5. The molecular orbitals and energy gaps between HOMO and LUMO orbitals and MEP map of compounds **3** and **4** in the **Azo**/**a**, **Azo**/**b** and **Hydrazo** forms, respectively, calculated by ωB97X-D/6-311G(d,p) method in NMF.

Table 7 Optimized parameters calculated by using ωB97X-D/6-311G(d,p) method of **Hydrazo** form of arylazo pyridone dyes in NMF.

Comp.	Interatomic distance (Å)					Torsion angle (°)	
	N2—H	N1—N2H	C5—N1	C6═O	C2═O	θ_1	θ_2
1	1.0219	1.2780	1.3210	1.2261	1.2180	89.993	0.005
2	1.0222	1.2764	1.3237	1.2268	1.2185	86.233	4.840
3	1.0227	1.2740	1.3273	1.2277	1.2192	86.456	5.385
4	1.0210	1.2882	1.3118	1.2237	1.2161	86.172	5.833
5	1.0221	1.2775	1.3217	1.2264	1.2180	89.848	0.056
6	1.0216	1.2804	1.3194	1.2257	1.2176	86.544	6.335
8	1.0218	1.2802	1.3191	1.2257	1.2176	85.616	4.395
9	1.0215	1.2812	1.3182	1.2253	1.2173	89.968	0.594
10	1.0215	1.2814	1.3189	1.2252	1.2173	89.990	0.009
11	1.0216	1.2814	1.3179	1.2254	1.2174	89.979	0.039

the largest bathochromic shift, and parabolic correlation was found for all compounds. Correlation results of the absorption maxima, ν_{max}, with calculated E_{gap} values are given in Table S9 and Fig. S10. These results are indirect evidence that **Hydrazo** forms predominate in most solvent used.

Correlations of the calculated dipole moments in NMF solvent with Hammett σ_p substituent constants are given in Fig. S11 and Eq. (S2). The high negative correlation coefficient indicates that electron-donating substituents contribute to an extensive π-delocalization with electron-deficient 2,6-pyridone structure (Fig. S5; structure **I**). This result is in accordance with correlation result μ *versus* σ (Fig. S11) and the highest values of coefficient s found in Kamlet–Taft correlations (Table S3). In electron-accepting substituted dyes two opposite electron-attracting effects exist causing decrease of the extent

Table 8 Calculated energies of the HOMO and LUMO orbitals and energy gaps for compounds **3** and **4** in NMF (**Hydrazo** form).

Compound	E_{HOMO} (eV)	E_{LUMO} (eV)	E_{gap} (eV)
1	−7.99	−1.21	6.78
2	−7.85	−1.18	6.67
3	−7.61	−1.15	6.46
4	−8.26	−1.57	6.69
5	−7.94	−1.21	6.73
6	−7.97	−1.27	6.70
8	−7.99	−1.26	6.73
9	−8.12	−1.28	6.84
10	−8.09	−1.28	6.81
11	−8.10	−1.28	6.82

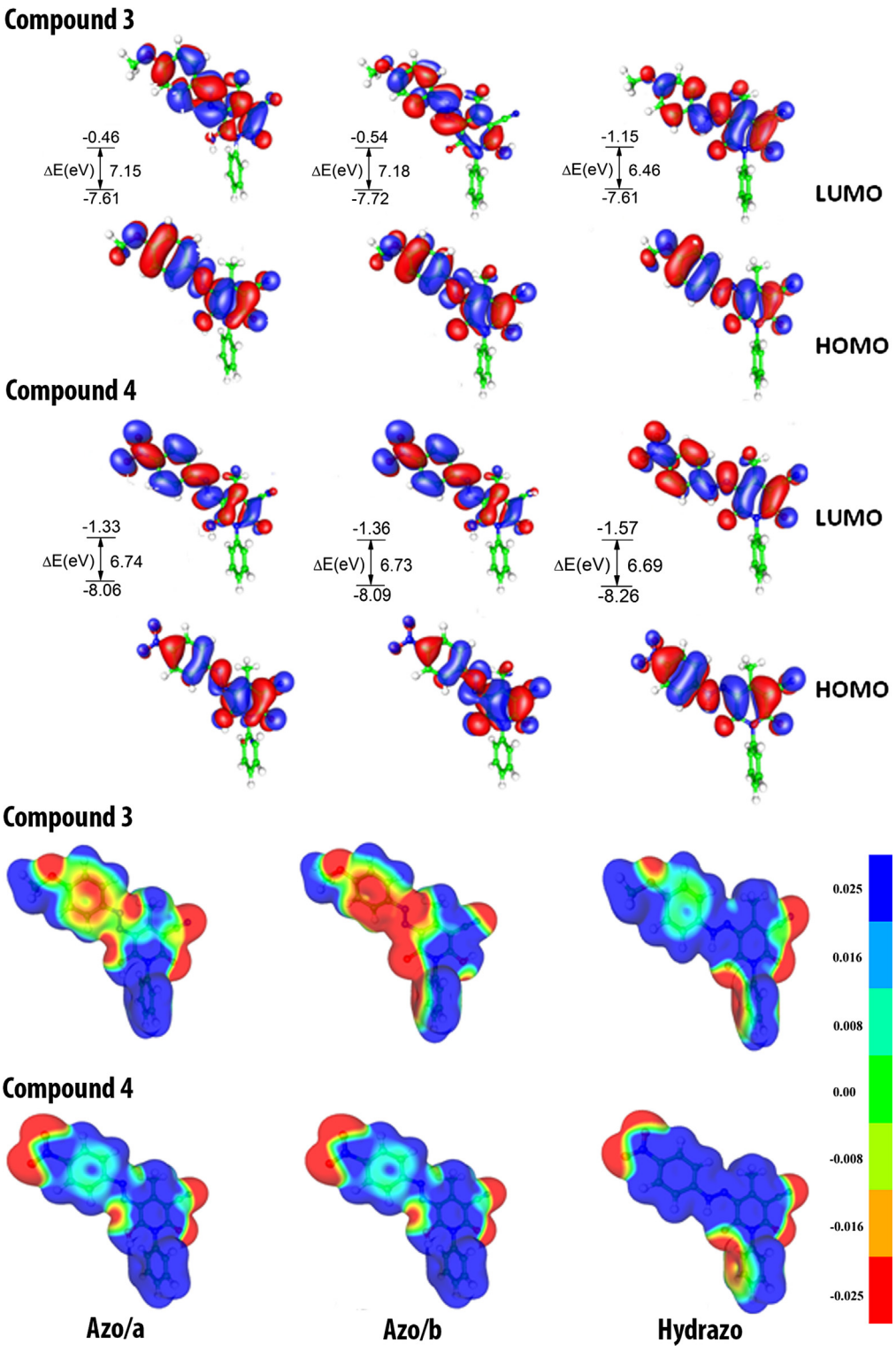

Figure 5 The molecular orbitals and energy gaps between HOMO and LUMO orbitals and MEP map of compounds **3** and **4** in the **Azo**/**a**, **Azo**/**b** and **Hydrazo** forms, respectively, calculated by ωB97X-D/6-311G(d,p) method in NMF.

of hydrogen bonding (Fig. S6; structure **VII**) which contributes to lower dipolarity of such structure (Table 6). The influence of the solvent permittivity, ε_r, on the absorption frequency, ν_{max}, is presented in Table S11, and low values of correlation coefficients indicate low sensitivity of absorption maxima to solvent dielectric capabilities.

MEP analysis was used to evaluate and visualize charge distribution over investigated compounds and illustrates the three dimensional charge distributions over all investigated molecules. MEP potential at a point in space around a molecule gives information about the net electrostatic effect produced at that point by total charge distribution (electron + proton)

of the molecule and correlates with dipole moments, electronegativity, partial charges and chemical reactivity of the molecules. It provides a visual method to understand the relative polarity of the molecule (Chidangil et al., 1998; Luque et al., 2000). An electron density isosurface mapped with electrostatic potential surface depicts the size, shape, charge density and site of chemical reactivity of the molecules. MEP shown in Figs. 5 and S12 illustrates the three dimensional charge distributions over all investigated molecules. As it is shown in Figs. 5 and S12, the different values of the electrostatic potential at the surface are represented by different colors; red represents regions of most electronegative electrostatic potential, and it indicates the region of high electron density, *i.e*. sites favorable for electrophilic attack; blue represents regions of the most positive electrostatic potential, *i.e*. region of low electron density favorable for nucleophilic attack, and green represents regions of zero potential. Potential increases in the order red < orange < yellow < green < blue. The blue color indicates the strong attractive potential, region favorable for HBA solvent interaction, while red color indicates the repulsive potential, and includes sites favorable for HBD solvent interactions. As it can be seen from the MEP map of the molecules, negative regions are mainly localized over the cyano and carbonyl groups attached at the pyridone rings and over the *nitro* substituent in compound **4**. The positive region is localized on the phenyl and pyridone rings. The negative potential of oxygen atoms oriented symmetrically in 2,6-positions of **Hydrazo** form, with respect to the central pyridone unit, is clearly visible in Figs. 5 and S12. Most of HBA capabilities of arylazo dyes could be assumed to be from 2,6-dioxo groups which are strong attractive electron-acceptor groups and cause increase of electron densities at these two sites creating favorable interaction with proton-donating solvents. HBD capabilities of solute molecule are mostly concentrated at azo pyridone moiety. As it can be seen from the MEP map of the compounds, the regions having the negative potential are over the electronegative atoms, the regions having the positive potential are over the phenylazo and pyridone rings and the remaining species are surrounded by zero potential.

Obviously, the ICT process is more feasible in NMF solvent. For compound **3**, the reason is higher planarity, while, in the case of compound **4**, higher rotation around the bond connecting the two electron-accepting groups can decouple the orbitals of these two groups providing medium for significant charge transfer. The highly polarizable ground and excited states of compounds **3** and **4** can be, under appropriate solvation conditions, preferentially stabilized by dipolar interactions. Due to this, the excited and ground states of compound **3** in **Hydrazo** form are closer and more rapid internal conversion is permitted.

The planar structure of investigated compounds supports conclusion that contribution of strong directional electronic transfer within two electronic structures: phenylazo and semi-aromatic pyridone ring is of high significance for electronic density transfer through overall compounds investigated. Structural diversity of studied compounds in different solvents depends on the contribution of the appropriate tautomeric form. Two oxygen atoms, present in **Hydrazo** form, show strong electron-accepting character of two keto groups (1,3-dicarbonyl structure in pyridone moiety). Electron-attracting power of two carbonyl groups in investigated molecules shifts more significantly electron densities from outer part of molecule. Compounds distinguishing from others are *meta*-substituted compounds which exert non-directional transmission of substituent effect that contributes even more that 1,3-diketo structure displaying larger electron-accepting character. In this way, *N*(1)-phenyl ring, due to lower n,π-resonance interaction, showed larger deviation from planarity providing higher accessibility of two keto groups to the stabilization by solvent hydrogen bonding interaction.

4. Conclusion

The UV–Vis and NMR data of eleven arylazo pyridone dyes were analyzed by the use of LSER and LFER principles. The K_T constants were estimated by using an advanced spectral data processing method based on the resolution of overlapping bands in UV–Vis spectra. The **Hydrazo** forms predominate in most solvents used. The solvatochromism of the dyes was analyzed with Kamlet–Taft model, and obtained results show that non-specific solvent effect is the main factor that influences the shift of absorption maxima. The introduction of electron-donating substituents in arylazo ring results in bathochromic shifts, while electron-accepting substituents showed appropriate alternation which depends on both substituent and molecular geometry.

The LFER analysis applied to ν_{max} implies that solvent effects have significant influence on the transmission mode of substituent effects. Positive solvatochromism was found mainly for protic solvents. The LFER analysis of *SCS* data shows reverse substituent effect, except for C5 atom which is the atom of the highest susceptibility to substituent effects.

Quantum chemical calculations indicate that substituents significantly change the extent of conjugation, and affect the ICT character of the investigated dyes. AIM analysis of ωB97X-D/6-311G(d,p) optimized structure of arylazo pyridone dyes displayed the presence of strong hydrogen bonding in **Hydrazo** form. The MEP map shows that regions with negative potential are over the electronegative oxygen atoms, oriented symmetrically in 2,6-positions of pyridone ring showing the highest HBA capabilities. On the other hand, the region with positive potential is over the phenylazo and pyridone rings showing most of HBD capabilities. Theoretical calculations and experimental results gave an insight into the influence of the molecular conformation on the transmission of substituent effects, as well as on contribution of different solvent–solute interactions.

Acknowledgment

The authors acknowledge the financial support of the Ministry of Education, Science and Technological Development of the Republic of Serbia (Grant No. 172013).

Appendix A. Supplementary material

Supplementary data associated with this article can be found, in the online version, at http://dx.doi.org/10.1016/j.arabjc.2015.08.029.

References

Ajaj, I., Markovski, J., Markovic, J., Jovanovic, M., Milcic, M., Assaleh, F., Marinkovic, A., 2014. Struct. Chem. 25, 1257–1270.

Ajaj, I., Mijin, D., Maslak, V., Brković, D., Milčić, M., Todorovic, N., Marinković, A., 2013. Monatsh. Chem. 144, 665–675.

Alimmari, A., Mijin, D., Vukićević, R., Božić, B., Valentić, N., Vitnik, V., Vitnik, Ž., Uščumlić, G., 2012. Chem. Cent. J. 6, 71.

Alimmari, A., Božić, B., Mijin, D., Marinković, A., Valentić, N., Uščumlić, G., 2013. Arab. J. Chem. http://dx.doi.org/10.1016/j.arabjc.2013.10.001.

Antonov, L., Stoyanov, S., 1993. Appl. Spectrosc. 47, 1030–1035.

Antonov, L., Stoyanov, S., 1995. Anal. Chim. Acta 314, 225–232.

Antonov, L., 2013. Tautomerism: Methods and Theories. Wiley-VCH, Weinheim.

Cee, A., Horáková, B., Lyčka, A., 1988. Dyes Pigm. 9, 357–369.

Chai, J.-D., Head-Gordon, M., 2008. Phys. Chem. Chem. Phys. 10, 6615–6620.

Chidangil, S., Shukla, M.K., Mishra, P.C., 1998. J. Mol. Model. 4, 250–258.

Ertan, N., Eyduran, F., Gurkan, P., 1995. Dyes Pigm. 27, 313–320.

Ertan, N., Gurkan, P., 1997. Dyes Pigm. 33, 137–147.

Exner, O., 1972. The Hammett equation – the present position. In: Champan, N.B., Shorter, J. (Eds.), Advances in Linear Free Energy Relationship. Plenum Press, London, pp. 1–69.

Frisch, M.J., Trucks, G.W., Schlegel, H.B., Scuseria, G.E., Robb, M. A., Cheeseman, J.R., Scalmani, G., Barone, V., Mennucci, B., Petersson, G.A., Nakatsuji, H., Caricato, M., Li, X., Hratchian, H. P., Izmaylov, A.F., Bloino, J., Zheng, G., Sonnenberg, J.L., Hada, M., Ehara, M., Toyota, K., Fukuda, R., Hasegawa, J., Ishida, M., Nakajima, T., Honda, Y., Kitao, O., Nakai, H., Vreven, T., Montgomery, Jr., J.A., Peralta, J.E., Ogliaro, F., Bearpark, M., Heyd, J.J., Brothers, E., Kudin, K.N., Staroverov, V.N., Kobayashi, R., Normand, J., Raghavachari, K., Rendell, A., Burant, J.C., Iyengar, S.S., Tomasi, J., Cossi, M., Rega, N., Millam, J.M., Klene, M., Knox, J.E., Cross, J.B., Bakken, V., Adamo, C., Jaramillo, J., Gomperts, R., Stratmann, R.E., Yazyev, O., Austin, A.J., Cammi, R., Pomelli, C., Ochterski, J.W., Martin, R.L., Morokuma, K., Zakrzewski, V.G., Voth, G.A., Salvador, P., Dannenberg, J.J., Dapprich, S., Daniels, A.D., Farkas, Ö., Foresman, J.B., Ortiz, J. V., Cioslowski, J., Fox, D.J., 2009. Gaussian Inc., Gaussian 09, Revision C.01, Wallingford, CT.

Geng, Y., Gu, D., Gan, F., 2004. Opt. Mater. 27, 193–197.

Hammett, L.P., 1937. J. Am. Chem. Soc. 59, 96–103.

Hansch, C., Leo, A., Hoekman, D., 1995. Exploring QSAR: hydrophobic, electronic and steric constants. ACS Professional Reference Book. American Chemical Society, Washington, DC.

He, J., Bian, S., Li, L., Kumar, J., Tripathy, S., Samuelson, L., 2000. J. Phys. Chem. B 104, 10513–10521.

Hosseinnezhad, M., Gharanjig, K., Moradian, S., Tafaghodi, S., 2019. Arab. J. Chem. 12, 2069–2076. http://dx.doi.org/10.1016/j.arabjc.2014.12.027.

Isak, S.J., Eyring, E.M., Spikes, J.D., Meekins, P.A., 2000. J. Photochem. Photobiol. A 134, 77–85.

Jain, R., Bally, T., Rablen, P.R., 2009. J. Org. Chem. 74, 4017–4023.

Johnson, E.R., Keinan, S., Mori-Sánchez, P., Contreras-García, J., Cohen, A.J., Yang, W., 2010. J. Am. Chem. Soc. 132, 6498–6506.

Kamlet, M.J., Abbound, J.L.M., Taft, R.W., 1981. An examination of linear solvation energy relationships. In: Taft, R.W. (Ed.), Progress in Physical Organic Chemistry, vol. 13. Wiley, New York, pp. 485–630.

Kamlet, M.J., Abboud, J.M., Abraham, M.H., Taft, R.W., 1983. J. Org. Chem. 48, 2877–2887.

Koch, U., Popelier, P.L.A., 1995. J. Phys. Chem. 99, 9747–9754.

Kolehmainen, E., Ośmialowski, B., Krygowski, T.M., Kauppinen, R., Nissinen, M., Gawinecki, R., 2000. J. Chem. Soc., Perkin Trans. 2, 1259–1266.

Li, Y., Chen, C., Hsu, Y., Hsu, H., Chi, Y., Chen, B., 2010. Tetrahedron 66, 4223–4229.

Lučka, A., Machaček, V., 1986. Dyes Pigm. 7, 171–185.

Luque, F.J., Lopez, J.M., Orozco, M., 2000. Theor. Chem. Acc. 103, 343–345.

Lu, T., Chen, F., 2012. J. Comp. Chem. 33, 580–592.

Manolova, Y., Deneva, V., Antonov, L., Drakalska, E., Mornekova, D., Lambov, N., 2014. Spectrochim. Acta A 132, 815–820.

Marenich, A.V., Cramer, C.J., Truhlar, D.G., 2009. J. Phys. Chem. B 113, 6378–6396.

Mijin, D., Uščumlić, G., Perišić-Janjić, N., Valentić, N., 2006. Chem. Phys. Lett. 418, 223–229.

Mohareb, R.M., Ibrahim, N.S., 1989. J. Prakt. Chem. 331 (3), 387–392.

Ortiz, S., Alvarez-Ros, M.C., Alcolea Palafox, M., Rastogi, V.K., Balachandran, V., Rathor, S.K., 2014. Spectrochim. Acta A 130, 653–668.

Peng, Q., Li, M., Gao, K., Cheng, L., 1990. Dyes Pigm. 14, 89–99.

Peng, Q., Li, M., Gao, K., Cheng, L., 1991. Dyes Pigm. 15, 263–274.

Petrov, V., Antonov, L., Ehara, H., Harada, N., 2000. Comput. Chem. 24, 561–569.

Reichardt, C., 2003. Solvents and Solvent Effects in Organic Chemistry, third ed. Wiley-VCH, Weinheim.

Shams, H.Z., Helal, M.H., Samir, I.M., Mohareb, R.M., 2008. Pigm. Res. Technol. 37 (5), 299–307.

Szyc, Ł., Guo, Yang, J.M., Dreyer, J., Tolstoy, P.M., Nibbering, E.T. J., Czarnik-Matusewicz, B., Elsaesser, T., Limbach, H.H., 2010. J. Phys. Chem. A 114, 7749–7760.

Tao, J., Mao, G., Daehne, L., 1999. J. Am. Chem. Soc. 121, 3475–3485.

Thanthiriwatte, K.S., Hohenstein, E.G., Burns, L.A., Sherrill, C.D., 2011. J. Chem. Theory Comput. 7, 88–96.

Tomasi, J., Mennucci, B., Cammi, R., 2005. Chem. Rev. 105, 2999–3093.

Tsuno, Y., Kusuyama, Y., Sawada, M., Fuji, T., Yukawa, Y., 1975. Bull. Chem. Soc. Jpn. 48, 3337–3346.

Uščumlić, G., Mijin, D., Vajs, V., Sušić, B., 2004. Chem. Phys. Lett. 397, 148–153.

Wang, P.Y., Wang, I.Y., 1990. Textile Res. J. 60, 519–524.

Yazdanbakhsh, M.R., Ghanadzadeh, A., Moradi, E., 2007. J. Mol. Liq. 136, 165.

Yen, M.S., Wang, I.J., 2004. Dyes Pigm. 61, 243–250.

Yuan, X.-X., Wang, Y.-F., Wang, X., Chen, W., Fossey, J.S., Wong, N.-B., 2010. Chem. Central J. 4, 6.

Zhang, G., Wang, S., Gan, Q., Zhang, Y., Yang, G., Ma, J., 2005. Eur. J. Inorg. Chem. 20, 186–192.

Zollinger, H., 2003. Color Chemistry: Synthesis, Properties and Application of Organic Dyes and Pigments, third ed. Wiley-VCH, Weinheim.